MINISTRY OF EDUCATION AND TRAINING

VIETNAM NATIONAL CHEMICAL GROUP

VIETNAM INSTITUTE OF INDUSTRIAL CHEMISTRY

PHAM THI HOA

SYNTHESIS OF Me-O-W (Me: Si, Ti, Zr) CATALYSTS AND INVESTIGATION OF ITS CATALYTIC ACTIVITIY FOR THE CONVERSION REACTION OF FRUCTOSE INTO 5-HYDROXYMETHYLFURFURAL

Specialty: Organic Chemistry

Chemistry Code: 9.44.01.14

SUMMARY OF DOCTORAL THESIS

Ha Noi, 2023

The thesis completed at:
Vietnam Institute of Industrial Chemistry

Scientific instructors:

1. **Assoc. Prof. Dr. Nguyen Thanh Binh**
   University of Science
   Vietnam National University, Hanoi
2. **Dr. Đang Thi Thuy Hanh**
   Vietnam Institute of Industrial Chemistry

Reviewer:

1. **Assoc. Prof. Dr. Doan Thi Mai Hương**
   Institute of Marine Biochemistry
   Vietnam Academy of Science and Technology
2. **Dr. of science Dang Thanh Tuan**
   University of Science
   Vietnam National University, Hanoi
3. **Assoc. Prof. Dr. Tran Thi Phuong Thao**
   Chemical institute
   Vietnam Academy of Science and Technology

A- INTRODUCTION

1. Rationale of the thesis

Today, cellulose comes from straw, sugarcane bagasse, and inexpensive, readily available non-food crops that are a source of raw materials to produce renewable fuel products or other chemicals. One of these conversion pathways is through a series of reactions from cellulose/lignocellulose hydrolysis to glucose, followed by isomerization of glucose to fructose, and from there to a catalytic three-water separation reaction. acid to produce 5-hydroxylmethylfurfural (5-HMF). The compound 5-HMF is considered one of the potential platform chemicals that can be used to produce a variety of products depending on the catalyst and reaction conditions.

The synthesis of 5-HMF from fructose occurs via a dehydration reaction with or without an acid catalyst. The acidity of the catalyst plays an important role in the fructose reduction reaction. Between homogeneous and heterogeneous acid catalysts, the homogeneous acid catalyst system can convert fructose into 5-HMF with high efficiency but has limitations such as not being able to recover the catalyst, corroding equipment and causing pollution. environment. The current new trend is to use heterogeneous acid catalyst systems due to advantages such as the ability to recover and reuse, is more environmentally friendly and can achieve high performance, especially product selectivity. . Recently, heterogeneous catalysts such as WO_3 are known as strong solid acid catalysts, with good catalytic performance in many organic reactions. Due to its low specific surface area, WO_3 catalyst is often synthesized as a carrier catalyst. Many studies have shown that WO_x structural forms and their dispersion on the support surface play an important role in catalytic performance. With the advantages and prospects of WO_3-based catalysts, in this thesis, we research the synthesis of solid acid catalyst systems such as Si-O-W, Ti-O-W, Zr-O-W using the sol gel method and Application for the reaction to create 5-hydroxymethylfurfural (5-HMF) from the starting material fructose, one of the important links in the process of creating biofuels and basic chemical compounds.

With the research orientation of synthesizing heterogeneous oxide catalysts using the sol gel method, and applying it to the above reaction, we hope to easily change the Me:W molar ratio (Me: Si, Ti, Zr) and will synthesize WO_3 oxide to better disperse in the mixture, to improve the catalytic efficiency for the reaction to create 5-HMF from

fructose. On the other hand, according to recently published documents, currently the synthesis of the above catalyst system by the sol gel method has not been studied much, and the Me:W molar ratio (Me: Si, Ti, Zr) and their application for the conversion of fructose to 5-HMF is still very limited. Therefore, in this thesis we hope to contribute to enriching the research results on solid acid catalytic systems Me-O-W (Me: Si, Ti, Zr) using the sol gel method with different ratios. Me:W molar ratio (Me: Si, Ti, Zr) is different.

2. Research objectives and contents

- The thesis aims to research the synthesis of solid acid catalyst Me-O-W (Me: Si, Ti, Zr) using the sol gel method with different molar ratios of Me:W (Me: Si, Ti, Zr) and applied to the reaction of converting fructose into 5-HMF. To achieve the goal, the thesis focuses on implementing the following main research contents:
- Research on the synthesis of Me-O-W catalyst (Me: Si, Ti, Zr) by sol gel method with different Me:W molar ratios (Me: Si, Ti, Zr) and determine the morphological characteristics Their ergonomics and structure.
- Research on the synthesis of MeO_2/WO_x (Me: Si, Ti, Zr) catalysts by impregnation method and determine their morphological and structural characteristics to compare with the above oxides.
- Evaluate the effectiveness of catalysts for the dehydration reaction of fructose into 5-HMF in order to compare and find catalysts with the highest 5-HMF production efficiency for each of the above catalytic systems.
- Research factors affecting reaction performance such as reaction temperature, time, initial fructose concentration.
- Compare the effectiveness of the above catalysts with MeO_2/WO_x catalysts (Me: Si, Ti, Zr) synthesized by impregnation method to highlight the effectiveness of the catalytic synthesis method by sol gel method.

3. The scientific and practice meaning of the thesis

The sol gel method to synthesize Me-O-W catalyst (Me: Si, Ti, Zr) with different molar ratios contributes to enriching solid acid catalyst synthesis methods for the 5-HMF reaction. from fructose. This synthesis method is easy to perform and provides high 5-HMF production efficiency, up to 95.8%, which shows the superiority of the catalyst compared to other heterogeneous acid catalysts.

The reaction to create 5-HMF from the starting material fructose also contributes to the further goal of going from other materials derived from biomass such as glucose and cellulose, to create valuable biological products. treat.

4. The new contributions of the thesis

- Me-O-W mixed oxide catalysts (Me: Zr, Ti, Si) with different Me/W ratios were successfully synthesized for the first time by sol-gel method with precursors WCl_6 and $ZrOCl_2$.
- Systematically studied the conversion of fructose into HMF over Me-O-W catalyst. The results show that the HMF formation efficiency is very high, especially on Zr_9W_1, reaching 95.8%. This result is superior to the catalyst synthesized by the Zr_9/W_1 impregnation method with the same molar ratio condition W: Zr= 1:9, reaching only 81.6%. This is also an outstanding result compared to other research results. Research has shown that the optimal conditions for the reaction are: reaction temperature 120^{o}C, reaction time 2.5% (kl) fructose in DMSO solvent with the presence of 100 mg of catalyst.
- Structural characterization studies have shown that WO_x nanoclusters with a diameter of 1-2 nm have been formed and dispersed quite evenly, without clumping into large particles when using the sol-gel method, especially especially on Zr_9W_1 catalyst. This is considered a structural form containing the main active centers for WO_x-based catalysis. This result is clearly shown when there is a rapid increase in the activity of the Me-O-W catalytic material when the W:Me molar ratio is at a small value. At the same time, the research also showed the advantage of forming nanocluster phases on the oxide base compared to the conventional impregnation method.

5. Layout of the thesis

The thesis includes 130 pages, 17 tables, 80 drawings and graphs, distributed into parts including: Introduction - 2 pages; Overview of theory - 40 pages; Experiments and research methods - 8 pages; Results and discussion - 51 pages; Conclusion - 2 pages; New contributions of the thesis - 1 page; List of published projects - 2 pages; References - 11 pages (138 references); Appendix - 13 pages.

B- MAIN CONTENT

CHAPTER 1: OVERVIEW

This chapter presents an overview of fructose and 5-HMF, the synthesis processes of 5-HMF from different raw materials and the factors affecting the synthesis process. The review also provides a

general introduction to heterogeneous acid catalysis for 5-HMF synthesis, catalysis based on WO_3, based on individual oxides and an overview of the mixed oxide material Me-O-W (Me: Si, Ti, Zr). Some catalytic synthesis methods such as sol gel method, impregnation method,...

CHAPTER 2 : EXPERIMENT

2.1. Chemistry

The chemicals used all met analytical purity: $ZrOCl_2.8H_2O$ 99% (China), $Ti(C_4H_9O)_4$ 99% (Sigma Aldrich), $Si(OC_2H_5)_4$ 99% (Sigmal aldrich), WCl_6 99 % (Merck), C_2H_5OH 99% (China), P123 (Sigma Aldrich), DMSO(Merck), N_2 gas 99%, Fructose (Sigma Aldrich).

2.2. Materials synthesis processes

2.2.1. Me-O-W material synthesis process (Me: Zr, Ti, Si)

Dissolve 1g P123 in 10 ml ethanol, stir vigorously until all solid dissolves. Then add to the above mixture the precursor solutions such as WCl_6 dissolved in C_2H_5OH 99% and one of the solutions $ZrOCl_2.8H_2O$, $Ti(C_4H_9O)_4$, $Si(C_2H_5O)_4$) in C_2H_5OH 99% solvent with different mole ratios. The mixture was stirred at room temperature for about 2 hours. After completing the stirring, the mixture was aged at 40^{o}C for 5 days, then dried at 60^{o}C for 24 hours to evaporate the solvent. Finally, the solid was calcined in air at 400^{o}C for 5h, with a heating rate of 1min/degree.

The catalytic materials Me-O-W or $Me_xW_{10-x}O_y$ have a molar ratio, in which x = 0, 1, 3, 5, 7, 9, 10. With x = 0 the catalyst is WO_3 and with x = 10 the catalyst is MeO_2.

2.2.2. Process for synthesizing WO_3/MeO_2 materials (Me: Zr, Ti, Si)

The catalytic material WO_3/MeO_2 (Me: Zr, Ti, Si) is synthesized by impregnation method according to the following steps: Weigh a quantity of MeO_2 catalyst (Me: Zr, Ti, Si) that has been synthesized according to the procedure. above process and WCl_6 99% in molar ratio 9:1 then add 10ml of ethanol solvent, stir the mixture for 2 hours. The mixture is dried at 40-60^{o}C for 24 hours to evaporate the solvent. Heating the solid at 400^{o}C for 3 hours with a heating rate of 1 minute/degree.

The catalysts WO_3/ZrO_2, WO_3/TiO_2, WO_3/SiO_2 are denoted as TZ9, TT9, TS9, respectively.

2.3. Me-O-W catalytic regeneration process (Me: Zr, Ti, Si)

The catalyst obtained after the reaction was filtered and centrifuged at 7000 rpm for about 5 minutes. The solid was separated, filtered, washed with water and ethanol and then dried at 70°C for 24 hours. The resulting catalyst was calcined at 400°C to clean the surface, then put into the reaction to convert fructose into 5-HMF according to the reaction conditions.

2.4. Characteristic methods for evaluating material properties

The structural and morphological characteristics of the catalytic materials are determined through modern physical methods such as: XRD, FTIR, SEM, TEM, STEM-HAADF, BET, TPD-NH_3, XPS.

2.5. Evaluate the conversion efficiency of the catalyst

The conversion efficiency of the catalyst was evaluated through the reaction of converting fructose into 5-hydroxymethylfurfural. The reaction system is carried out in a three-necked flask connected to a spiral condenser. The process of a typical catalytic activity evaluation process is as follows: put 100 mg of catalyst into the reaction vessel and activate at 120°C in N_2 gas flow for 1 hour (200 ml/min). Next, add 10 ml of DMSO solvent containing 5% fructose into the flask; Continuously stir the reaction mixture at the investigation temperature of 120°C for 2 h, under N_2 gas environment. Cool the solution quickly after the reaction with cold water. Separate the product from the catalyst sample using a 45 µm filter.

In survey experiments, the role, reaction conditions, temperature parameters, time, fructose concentration and solvent can be changed.

The reaction efficiency is calculated through the formula:

$$H\% = \frac{C\,(ppm)}{Co\,(ppm)} x100\%$$

In particular, the resulting 5-HMF concentration (ppm) was determined according to the standard curve extrapolation method, by measuring HPLC high-performance liquid chromatography spectroscopy of solutions after the dehydration reaction of fructose to 5-HMF.

CHAPTER 3. RESULTS AND DISCUSSION

3.1. Si-O-W catalytic material

3.1.1. Characteristic results of Si-O-W materials

To determine the oxide formation temperature, TGA thermal analysis method was used for sample Si_5W_5. The minimum calcination temperature chosen is 400°C.

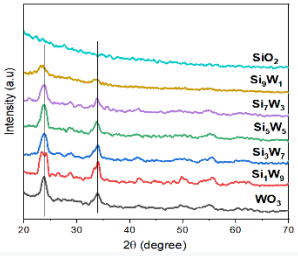

Figure 3.1. XRD patterns of WO_3, SiO_2 and Si-O-W

In the XRD diagram Figure 3.1 of SiO_2 material, SiO_2 material exists in amorphous form, the remaining materials all have a crystalline structure with peaks characteristic of the monoclinic phase structure of WO_3. Peak intensity at angles $2\theta \sim 23.1^o$ and 33.5^o of Si_9W_1 is much weaker than other Si-O-W samples, proving that Si_9W_1 has less crystallinity of WO_3 phase, possibly due to low WO_3 content, creating peaks with weak intensity.

The FTIR spectra of all samples showed signals at 3500 cm^{-1} that characterized the vibrations of the –OH group in water molecules adsorbed on the catalyst surface and the signal at 1646 cm^{-1} was assigned to deformation vibrations of Si–OH groups. Sample WO_3 shows absorption peaks at wave numbers 931, 822, 764 cm^{-1}, which characterize the vibrations of the W-O bond.

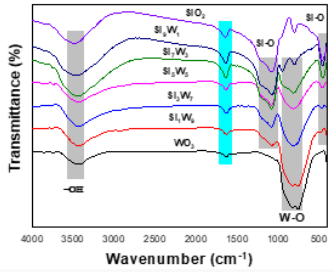

Figure 3.2. FTIR spectra of SiO_2, WO_3 and Si-O-W

On the IR spectrum of SiO_2, there are vibrations of Si–O groups at wave numbers 1224, 1084 cm^{-1}. The vibration at wavenumber 804 cm^{-1} was assigned to the bending vibration of Si–O–Si groups. The vibration at wavenumber 462 cm^{-1} is assigned to the deformation vibration of Si–O groups. The FTIR spectrum of the Si-O-W oxide mixture shows the superposition of the absorption peaks of the vibrations of the Si-O and W-O groups.

TEM images of Si_5W_5 and Si_9W_1 materials (Figure 3.3) show that Si-O-W materials are spherical in shape, the particles are small (20-30 nm), and the particle size is quite uniform.

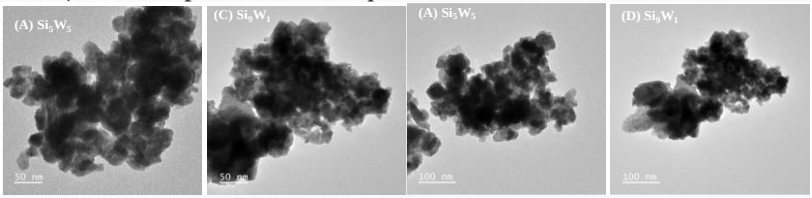

Figure 3.3. TEM images of material samples Si_5W_5 and Si_9W_1 (A), (B) Si_5W_5 and (C), (D) Si_9W_1

The results of elemental analysis are presented in Figure 3.4 and Table 3.1. Table 3.1 shows the elemental composition, percentage composition by mass and percentage composition by number of atoms in the compound. The ratio of Si/W atoms is 32.95/3.33, which is approximately the ratio 9/1, showing that the reagent Si_9W_1 has been synthesized in the correct ratio.

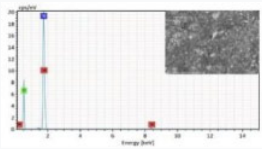

Figure 3.4. SEM-EDX measurement results of sample Si_9W_1

Table 3.1. Catalyst sample composition Si_9W_1

Ingredient	%Mass	%Atom
O	34.05	63.72
Si	30.91	32.95
W	20.46	3.33

Figure 3.5 shows the N_2 adsorption isotherm of sample Si_9W_1 of type IV, classified according to IUPAC. The N_2 adsorption-desorption isotherm at the relative pressure ratio P/Po = 0.45-1 displays a large hysteresis loop typically observed for mesoporous materials.

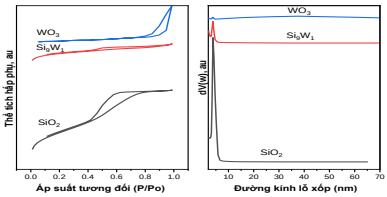

Figure 3.5. N_2 adsorption-desorption isotherm and capillary distribution curve of Si_9W_1

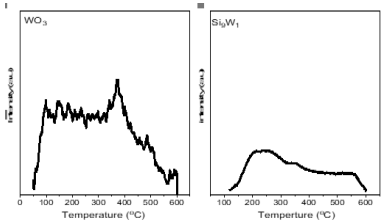

Figure 3.6. TPD-NH_3 diagram of WO_3 and Si-O-W materials

The synthesis of Si-O-W materials has increased the surface area parameters of the material system compared to single oxide WO_3. The TPD-NH_3 desorption curve of W-O-Si samples is presented in Figure 3.6. The TPD-NH_3 diagram was recorded at temperatures of 50-600°C.

Table 3.2. Measurement results Adsorption - desorption of N_2 and TDP-NH_3 of samples WO_3 and Si_9W_1

Material	S_{BET} (m^2/g)	V_{pore} (cm^3/g)	D_{BJH} (nm)	NH_3 (mmol/g catalysis)			
				Weak acid (150-300°C)	Medium acid (300-500°C)	Strong acid (> 500°C)	Total acid
WO_3	25.5	0,170	30,50	0,131	0,169	0,008	0,308
Si_9W_1	173,4	0,046	4,33	0.415	0.297	0.122	0,785

Si_9W_1 material shows significantly higher NH3 desorption capacity than WO_3 sample. The presence of well-dispersed WO_3 clusters on SiO_2 produces a higher number of weak to moderate and strong acidic sites. This fact shows that the introduction of WO_3 into the SiO_2 structure leads to a significant increase in the concentration of medium and weak acid centers, contributing to improving the catalyst activity. Especially the acid centers in the weak and medium acid centers are in the form of Bronsted acid centers as previously reported.

Information on the surface valence of Si_9W_1 material was analyzed by high-resolution spectroscopy (XPS) of W4f (36 eV), Si2p (104 and 155 eV) and O1s (535 eV). In Figure 3.7B, the O1s spectrum of Si9W1 material appears two maximum peak intensities at the binding energy 531.17; 533.09 and 533.97 eV can be assigned to the oxygen in

the M-O bonds (Si-O and W-O) and the O2- bond adsorbed on the catalyst surface.

The Si 2p high-resolution XPS spectrum of the Si-O-W material (Figure 3.7C) shows signals at 103.86 eV related to Si 2p. Similarly, the high-resolution spectrum of W4f of material Si_9W_1 (Figure 3.9D) shows signals at 35.28; 37 eV corresponding to $W4f_{7/2}$ and $4f_{5/2}$ characterizes the W^{5+} state, while the signals at 36.05; 38.13 characterizes the W^{6+} state. The appearance of the W^{5+} oxidation state is expected as the structure contains Bronsted acid sites (W^{5+}-OH) instead of Lewis acid sites (W^{6+}=O). Bronsted acid centers are considered to play a key role in the dehydration of fructose molecules into 5-hydroxymethylfurfural.

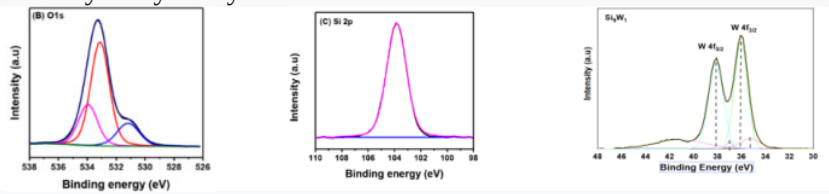

Figure 3.7. XPS spectrum of O1s(B); Si 2p (C) and W4f (D) of Si_9W_1

3.1.2. Evaluation of the activity of Si-O-W catalyst

The effectiveness of Si-O-W catalysts and the influence of temperature on the reaction efficiency of converting fructose into 5-HMF are presented in Figures 3.8 and 3.9.

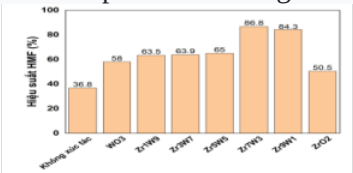

Figure 3.8. Effect of Si-O-W catalyst system on 5-HMF formation efficiency

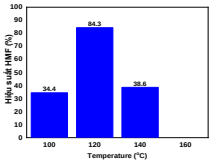

Figure 3.9. Effect of temperature on 5-HMF formation efficiency on Si_9W_1

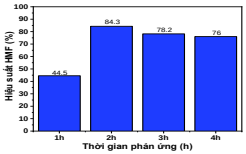

Figure 3.10. Effect of time

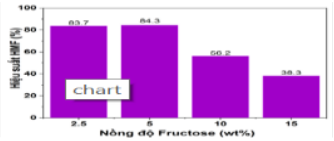

Figure 3.11. Effect of fructose concentration

In Figure 3.8, it is easy to see that the oxide catalysts Si_7W_3 and Si_9W_1 are the most active catalysts in the Si-O-W material samples with conversion efficiency to 5-HMF of about 86.8, respectively. % and 84.3%, much higher than the reaction without catalyst. From the perspective of 5-HMF performance and economic efficiency, the Si9W1 model was selected for further research.

Si9W1 material is used as a catalyst to convert fructose into 5-HMF when investigating different reaction conditions such as: temperature, reaction time, fructose concentration, reaction solvent is dimethylsulfoxide (DMSO).

The optimal reaction conditions for the reaction to create 5-HMF from fructose on the Si-O-W catalyst system are: reaction temperature 120^oC, reaction time 2h, initial fructose concentration 5% by weight.

When increasing time or fructose concentration, the efficiency decreases, possibly because the 5-HMF formed during the reaction continues to be hydrolyzed into levulinic acid (LA) and formic acid (FA), or because of the rate of hydrolysis. The conversion rate of 5-HMF into humin is higher than the reaction rate converting fructose into 5-HMF. The catalyst can be reused 3 times with almost no change in HMF product performance. This proves that the synthesized Si_9W_1 catalyst is a highly effective, sustainable catalyst with no change in activity during the conversion reaction.

3.2. Ti-O-W catalytic material

3.2.1. Characteristic results of Ti-O-W materials

XRD results of TiO_2, WO_3 and Ti-O-W samples are presented in Figure 3.12. In Figure 3.12, the peaks are at angle 2θ ~ 23.1; 26.4; 28.6; 33.4; 33.5; 41.3; 49.7 and 55.6o with high intensity characterize the monoclinic phase structure of WO_3 in the sample and Ti_1W_9, respectively.

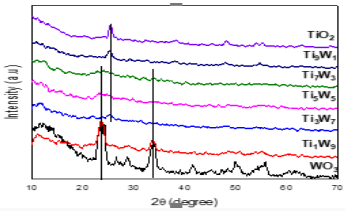

Figure 3.12. XRD patterns of WO_3, TiO_2 and Ti-O-W

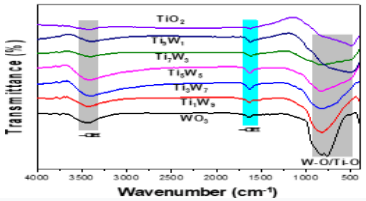

Figure 3.13. FTIR spectra of WO_3, TiO_2 and Ti-O-W

The XRD patterns of TiO_2 and Ti_9W_1 samples observed the anatase crystalline phase of TiO_2 with peaks at $2\theta \sim 25.3°$, 37.5°, 48° and 55°. On the XRD diffraction patterns of Ti_xW_{10-x} mixed oxides, it shows the superposition of diffraction peaks between the two phases WO_3 and TiO_2.

FTIR diagram Figure 3.13, the vibrations at 3200-3600 cm^{-1} are assigned to the vibrations of –OH groups due to water molecules adsorbed on the material surface. The frequency at wavenumber 1626 cm^{-1} is the bending vibration of the –OH group in the water molecule. The FTIR infrared spectrum of sample WO_3 shows absorption peaks at wave numbers 931, 822, 764 cm^{-1}, which characterize the vibrations of the W-O bond. Vibrations at wavenumbers of 500-800 cm^{-1} characterize the Ti–O bond of the TiO_2 phase. The FTIR spectrum of the oxide mixture shows superposition of the absorption peaks of the vibrations of the W-O and Ti-O groups.

SEM images of TiO_2 and Ti-O-W materials shown in Figure 3.14 show that Ti-O-W materials have agglomeration with a basic spherical shape and fairly uniform size.

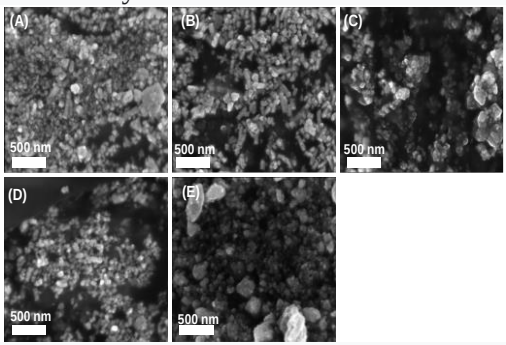

Figure 3.14. SEM images of Ti-O-W materials Ti_1W_9, (B)Ti_3W_7, (C) Ti_5W_5, (D) Ti_7W_3, and (E) Ti_9W_1

In Figure 3.15, TEM images of material samples Ti_5W_5 and Ti_9W_1 have spherical TiO_2 and WO_3 nanoparticles, with a particle size of about 10 nm, and the particles are quite uniform.

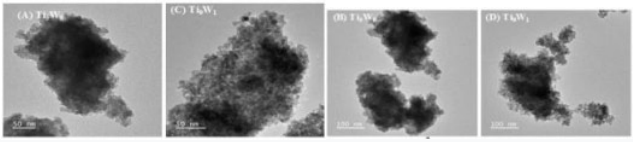

Figure 3.15. TEM images of Ti-O-W materials, (A), (B) Ti_5W_5 and (C), (D) Ti_9W_1

The results of elemental analysis are presented in Figure 3.16 and Table 3.3.

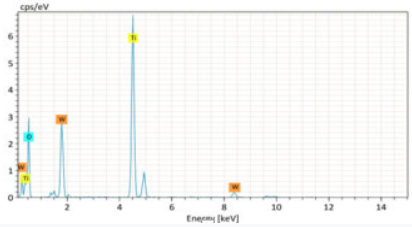

Figure 3.16. SEM-EDX spectrum of sample Ti_9W_1

Table 3.3. Composition of Ti_9W_1 catalyst sample

Ingredient	Mass (%)	Atom (%)
O	26.44	60.83
Ti	46.46	35.73
W	17.18	3.44

Table 3.3. Indicates the elemental composition, percentage composition by mass and percentage composition by number of atoms in the compound. The ratio of Ti/W atoms is 35.73/3.44, which is approximately the ratio of 9/1, showing that the Ti_9W_1 catalyst has been synthesized in the correct ratio.

The N_2 adsorption and desorption isotherm and pore size distribution curve of Ti-O-W material are presented in Figure 3.17, TPD-NH_3 diagrams of WO_3 and Ti_9W_1 are presented in Figure 3.18.
Figure 3.17 and table 3.4 show that the inclusion of WO_x phase and TiO_2 structure in the sample has significantly increased the surface area and pore volume parameters of the material. This is very favorable for increasing the number of active centers on the catalytic surface.

The Ti_9W_1 material in Figure 3.18 and Table 3.4 shows a significantly higher NH_3 desorption capacity than the WO_3 sample. The presence of well-dispersed WO_3 clusters on TiO_2 produces a higher number of weak-moderate to strong acidic sites. This result shows that

the introduction of WO_3 into the TiO_2 structure leads to a significant increase in the concentration of acid centers, contributing to improving the catalyst activity.

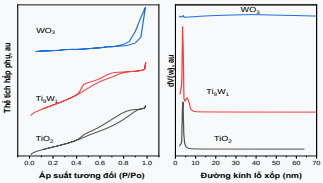

Figure 3.17. N_2 adsorption-desorption isotherm of WO_3, Ti_9W_1 and TiO_2

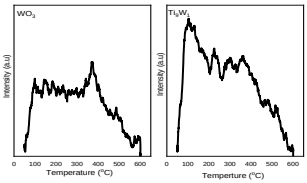

Figure 3.18. TPD-NH_3 diagram of WO_3 and Ti_9W_1

Table 3.4. Amount of NH_3 desorbed at different temperatures of WO_3 and Ti_9W_1 samples

Material	S_{BET} (m^2/g)	V_{pore} (cm^3/g)	D_{BJH} (nm)	NH_3 (mmol/$g_{catalysis}$)			
				Weak acid (150-300°C)	Medium acid (300-500°C)	Strong acid (>500°C)	Total acid
WO_3	25,5	0,170	30,50	0,131	0,169	0,008	0,308
Ti_9W_1	148,4	0,144	3,89	0,303	0,217	0,059	0,579

Information about the valence of elements at the surface of Ti_9W_1 material was analyzed by XPS spectrum.

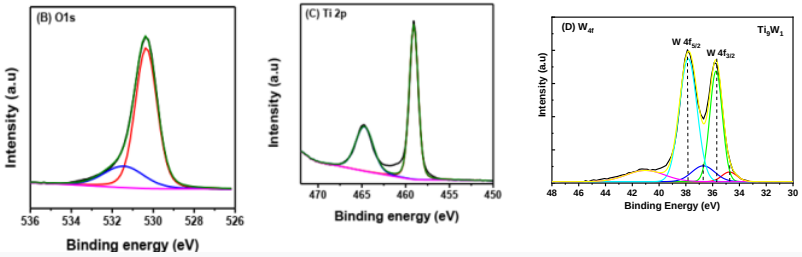

Figure 3.19. XPS spectrum of O1s (B); Ti2p (C) and W4f (D) of Ti_9W_1

In Figure 3.19, the high-resolution spectra W4f (38 eV), Ti2p (460 eV), and O1s (533 eV) are presented. In Figure 3.19B, the O1s spectrum of the Ti-O-W material appears two maximum peak intensities at the binding energies of 530.35 eV and 531.42 eV that can

be assigned to Oxygen in the M-O (Ti- O and W-O) and the O2- bond are adsorbed on the catalyst surface. The high-resolution spectrum of Ti2p (Figure 3.19C) shows signals at 459.08 eV and 464.74 eV associated with Ti2p. Similarly, the high-resolution spectrum of W4f of W-O-Ti material (Figure 3.19D) shows signals at 35.74; 37.82 eV related to $W4f_{7/2}$ and $4f_{5/2}$ characterizes W^{6+} and the signals at 34.75; 36.70 eV characterizes W^{5+}.

3.2.2. Evaluation of the activity of the Ti-O-W catalyst

The effect of W content (or W:Ti molar ratio) in Ti-O-W catalyst on the efficiency of fructose conversion into 5-HMF product is presented in Figure 3.20.

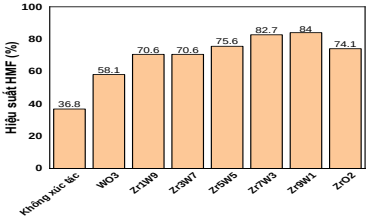

Figure 3.20. Effect of W:Ti ratio in Ti-O-W catalyst on the performance of 5-HMF product formation

In Figure 3.20, it can be seen that when the W:Ti ratio decreases, the 5-HMF generation efficiency increases clearly, reaching the highest 84% corresponding to Ti_9W_1.

This can be explained that a small amount of well-dispersed WO_3 on the surface of TiO_2 can create a resonance phenomenon between the two phases, thus increasing the efficiency of converting fructose into 5-HMF. From the results obtained, Ti_9W_1 catalyst was selected for further studies.Factors affecting the reaction efficiency of creating 5-HMF from fructose on Ti_9W_1 catalyst in DMSO solvent include: temperature, time, concentration.

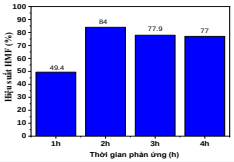

Figure 3.21. Effect of time

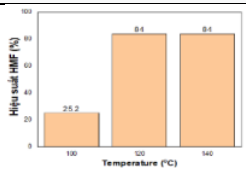

Figure 3.22. Effect of temperature

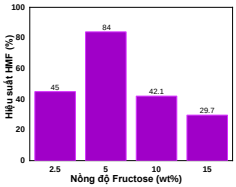

Figure 3.23. Effect of concentration

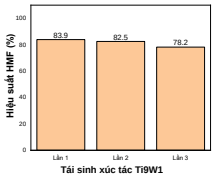

Figure 3.24. Durability of Ti_9W_1 catalyst

The optimal reaction conditions for the reaction to create 5-HMF from fructose on the Si-O-W catalyst system are: reaction temperature 120°C, reaction time 2h, initial fructose concentration 5% by weight.

The catalyst is highly effective and sustainable after 3 reuses.

3.3. Zr-O-W catalytic material

3.3.1. Characteristic results of Zr-O-W materials

Similar to the Si-O-W and Ti-O-W catalytic systems, to create the Zr-O-W oxide phase, the expected minimum calcination temperature is 400°C. XRD results of ZrO_2, WO_3 and Zr-O-W are presented in Figure 3.25.

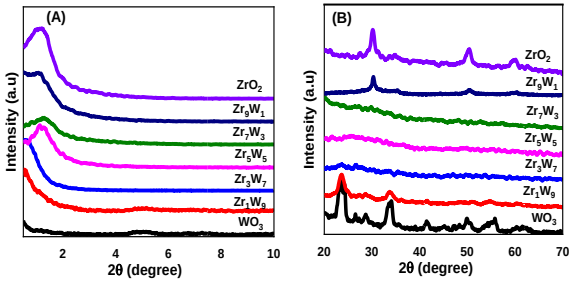

Figure 3.25. Narrow-angle (A) and wide-angle (B) XRD diagrams of WO_3, ZrO_2 and Zr-O-W material samples

In Figure 3.25A, the narrow-angle XRD diagram of material samples Zr_5W_5, Zr_7W_3, Zr_9W_1, ZrO_2 appears a peak at an angle of 2θ ~ 1.2°, typical of porous materials with a medium capillary structure. Thus, the use of surfactant P123 in the synthesis process has created a medium-porous, porous structure material. The wide-angle XRD pattern (Figure 3.25B) of ZrO_2 material shows peaks at an angle of 2θ ~ 30.2; 49.8 and 60.0° characterize the tetragonal phase of ZrO_2 oxide. This shows that zirconia-tungsten calcination leads to the formation of

a tetragonal phase of ZrO_2 that is more dominant than the monoclinic phase. WO_3 material shows the appearance of peaks characteristic of the monoclinic phase structure of WO_3 at the angle 2θ ~ 23.1; 26.4; 28.6; 33.4; 33.5; 41.3; 49.7 and 55.6°. In addition, the XRD pattern of mixed oxide ZrO_2 and WO_3 (Zr_3W_7, Zr_5W_5, Zr_7W_3) does not show the appearance of peaks typical for the tetragonal phase of ZrO_2 oxide and the monoclinic phase of WO_3. This may be due to the mixed oxides Zr_xW_{10-x} (x: 3,5,7,9) existing in microcrystalline and amorphous structures.

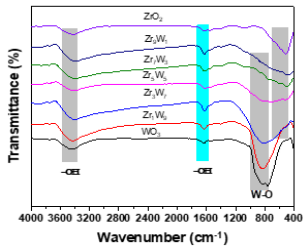

Figure 3.26. FTIR spectra of ZrO_2, WO_3 and Zr-O-W

In Figure 3.25A, the narrow-angle XRD diagram of material samples Zr_5W_5, Zr_7W_3, Zr_9W_1, ZrO_2 appears a peak at an angle of 2θ ~ 1.2°, typical of porous materials with a medium capillary structure. Thus, the use of surfactant P123 in the synthesis process has created a medium-porous, porous structure material.

The wide-angle XRD pattern (Figure 3.25B) of ZrO_2 material shows peaks at an angle of 2θ ~ 30.2; 49.8 and 60.0° characterize the tetragonal phase of ZrO_2 oxide. This shows that zirconia-tungsten calcination leads to the formation of a tetragonal phase of ZrO_2 that is more dominant than the monoclinic phase. WO_3 material shows the appearance of peaks characteristic of the monoclinic phase structure of WO_3 at the angle 2θ ~ 23.1; 26.4; 28.6; 33.4; 33.5; 41.3; 49.7 and 55.6°. In addition, the XRD pattern of mixed oxide ZrO_2 and WO_3 (Zr_3W_7, Zr_5W_5, Zr_7W_3) does not show the appearance of peaks typical for the tetragonal phase of ZrO_2 oxide and the monoclinic phase of WO_3. This may be due to the mixed oxides Zr_xW_{10-x} (x: 3,5,7,9) existing in microcrystalline and amorphous structures.

In Figure 3.27, the TEM image of the Zr-O-W material has a spherical shape, the particles are small in size (5-10 nm), and quite homogeneous. TEM images show that the Zr_9W_1 catalyst is formed from the agglomeration of spherical nanoparticles with diameters ranging from about 5 to 10 nm.

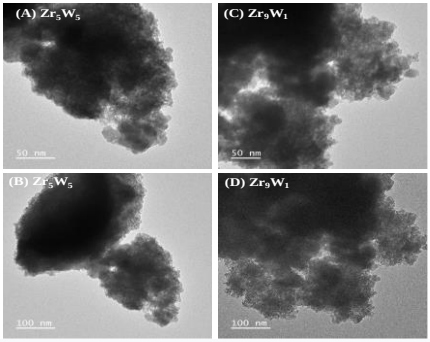

Figure 3.27. TEM images of Zr-O-W material samples (A), (B) Zr_5W_5 and (C), (D) Zr_9W_1

This result seems to be consistent with its wide-angle XRD pattern observed when the sample has poor crystallinity of the ZrO_2 tetrahedral phase. To further clarify the surface microstructure of the catalyst, HAADF imaging was also performed on the Z_9W_1 catalyst. It was found that there were bright dots or bright areas at nanoscale on the sample surface, corresponding to WO_x nanoclusters encapsulated by ZrO_2 carrier via oxygen bridge bond. In the STEM–HAADF image, the bright spots have diverse diameters from about 1 nm, corresponding to different sizes of the WO_x nanoclusters. Additionally, many of the bright nanoscale areas observed are due to WO_x nanoclusters.

The STEM – mapping image shows that W is uniformly distributed on the catalyst surface. This can confirm the advantage of the sol-gel method in this study, allowing it to avoid granular or polytungstate clustered WO_x phase, reducing the number of catalytic centers in the WO_x-based catalyst.

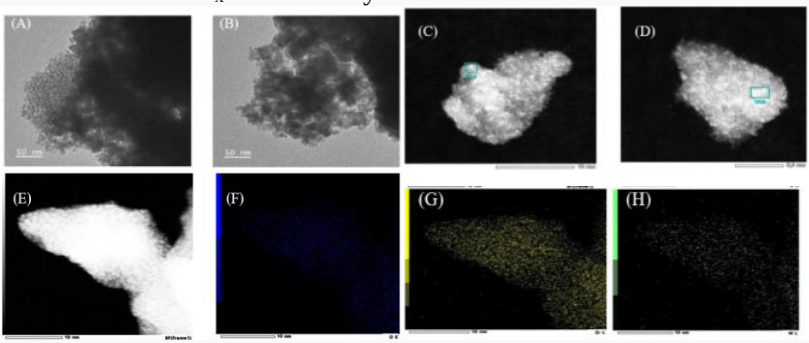

Figure 3.28. TEM images (A, B), HAADF(C,D) and STEM-MAPPING (E, F, G, H) of material sample Zr_9W_1

Zr-O-W material samples were also analyzed for elemental composition using the SEM-EDS method. Figure 3.29 presents the EDS results of the Zr_5W_5 material sample. Table 3.5 shows that there is not much difference in the Zr/W molar ratio between theoretical calculations and experimental results measured by the EDS method.

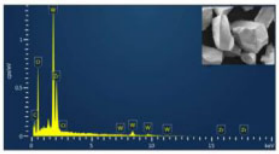

Figure 3.29. SEM-EDX measurement results of sample Zr_5W_5

Table 3.5. Zr/W molar ratio of Zr-O-W materials

Sample	Zr/W ratio (theoretical)	Zr/W ratio (experimental)
Zr_5W_5	1,00	1,00
Zr_3W_7	0,49	0,43
Zr_1W_9	0,08	0,11

The N_2 adsorption and desorption isotherms and pore size distribution curves of ZrO_2 and Zr-O-W materials are presented in Figure 3.30. The specific surface area (SBET), pore volume (Vpore) and pore distribution of ZrO_2, WO_3 and Zr-O-W samples are shown in Table 3.6. Observing the results obtained on the summary table, it can be seen that when the W content in the Zr-O-W mixed oxide decreases, the specific surface area increases and reaches the maximum value at S_{BET} = 106 m^2 for Zr_9W_1. It seems to be consistent with the poor crystallinity behavior of the mixed oxide. This change can be explained by the presence of the ZrO_2 phase that prevents the growth of WO_3 crystal nuclei.

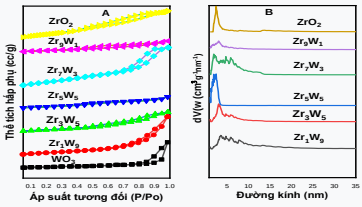

Figure 3.30. (A) Isotherm N2 adsorption-desorption and (B) capillary distribution curve of Zr-O-W

Table 3.6. Physicochemical parameters of ZrO_2, WO_3 and Zr-O-W.

STT	Material	S_{BET} (m^2/g)	D_{pore} (nm)	V_{pore} (cm^3/g)
1	WO_3	25,5	30,5	0,17
2	Zr_1W_9	61,7	7,04	0,18
3	Zr_3W_7	51,4	6,08	0,1
4	Zr_5W_5	98,2	4,88	0,08
5	Zr_7W_3	94,4	3,78	0,19
6	Zr_9W_1	106,4	5,20	0,14
7	ZrO_2	40,3	4,88	0,08

Table 3.7. Amount of NH_3 desorbed at different temperatures of WO_3, Zr_9W_1

Material	S_{BET} (m^2/g)	V_{pore} (cm^3/g)	D_{BJH} (nm)	NH_3 (mmol/$g_{catalysis}$)			
				Weak acid (150-300°C)	Medium acid (300-500 °C)	Strong acid (>500 °C)	Tổng lượng tâm acid
WO_3	25,5	0,170	30,50	0,131	0,169	0,008	0,308
Zr_9W_1	148,4	0,144	3,89	0,333	0,401	0,035	0,769

In Table 3.7, the amount of NH_3 desorbed at different temperatures of samples WO_3 and Zr_9W_1 is presented. Table 3.7 shows that the NH_3 desorption capacity of Zr_9W_1 is significantly higher than that of the WO_3 sample. This fact shows that the introduction of WO_3 into the ZrO_2 structure leads to a significant increase in the concentration of medium and weak acid centers, contributing to improving the catalyst activity.

W4f XPS spectrum shows peaks at binding energies of 35.94, 38.31 eV corresponding to orbitals $W^{6+}4f_{7/2}$, $W^{6+}4f_{5/2}$ and 35.8; 37.75 eV corresponding to orbitals $W^{5+}4f_{7/2}$, $W^{5+}4f_{5/2}$. This shows the coexistence of Lewis and Bronsted acid sites, corresponding to oxidation states W^{6+} and W^{5+}.

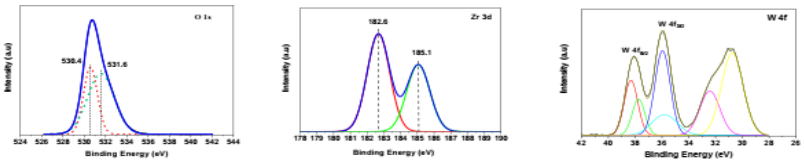

Figure 3.31. XPS spectrum of O1s; W4f and Zr3d of model Zr_9W_1.

3.3.2. Evaluation of the activity of the Zr-O-W catalyst system

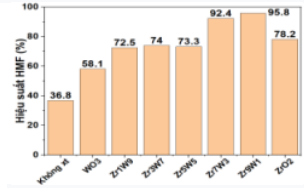

Figure 3.32. Effect of Zr-O-W ratio on 5-HMF generation efficiency

Figure 3.32 shows that when reducing the WO_3 content on the ZrO_2 carrier, the 5-HMF production efficiency increases clearly. In particular, the Zr_7W_3 and Zr_9W_1 catalysts showed significantly higher conversion efficiency of fructose to 5-HMF than other Zr-O-W catalysts and with ZrO_2 and WO_3 alone.

A small amount of WO_3 well dispersed on the surface of ZrO_2 creates a resonance phenomenon between the two elements, resulting in increased efficiency.

Furthermore, the tetrahedral form of ZrO_2 bonded to the octahedral [WO_6] structure can create defects leading to an increased number of bronsted acid centers. From the above results, it can be seen that the simultaneous combination of metal oxides ZrO_2 and WO_3 improved the reaction efficiency of converting fructose into 5-HMF. Thus, the Zr_9W_1 catalyst gives the best efficiency in converting fructose into 5-HMF product, reaching 95.8%. This catalyst was also selected for further studies on the effects of temperature, time, and concentration on the reaction performance of creating 5-HMF from fructose.

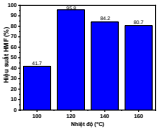

Figure 3.33. Effect of temperature

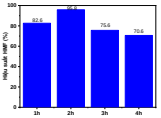

Figure 3.34. Effect of time

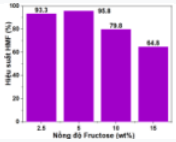

Figure 3.35. Effect of concentration

From the pictures above, it can be seen that the optimal survey conditions are: 120°C, 2h, fructose concentration 5% by weight. Changing the above conditions can lead to increased production of humin, or other byproducts, thereby reducing reaction efficiency.

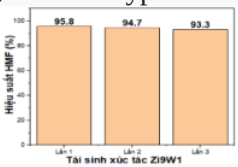

Figure 3.36. Stability of Zr_9W_1 catalyst in the reaction to create 5-HMF from fructose

Figure 3.36 shows that after 3 reuses, the product creation efficiency has not changed much, still approximately 95%. This proves that the synthesized Zr_9W_1 catalyst is a highly effective, sustainable catalyst that does not change activity in the conversion reaction.

3.4. Comparing the performance of Me_9W_1 materials (Me: Si, Ti, Zr)

3.4.1. General introduction

The catalytic materials Me-O-W or Me_xW_{10-x} (Me: Si, Ti, Zr; x = 0, 1, 3, 5, 7, 9, 10) have been synthesized by the solgel method and their structures determined. structure using modern analytical methods.

All catalytic materials showed acidity in the dehydration reaction of fructose to 5-HMF and all showed higher 5-HMF synthesis efficiency than the case without using catalyst. In each of the above oxide series, the catalytic activity of the samples gradually increases with x and reaches very high efficiency values with the Me_9W_1 samples. Those are three typical catalytic materials of the above three metal oxide series. In this section, we present the differences in morphological and surface properties of Me_9W_1 material leading to differences in the performance of 5-HMF synthesis from fructose.

3.4.2. Results of X-ray diffraction (XRD) characteristics of Me_9W_1 material (Me = Si, Ti, Zr).

The microcrystalline structures of materials Si_9W_1, Ti_9W_1, Zr_9W_1 are shown on wide-angle X-ray diffraction spectra. In Figure 3.37A, the XRD spectrum of Si_9W_1 has peaks characteristic of the monoclinic phase of WO_3, while Ti_9W_1 and Zr_9W_1 only show peaks characteristic of the anatase phase of TiO_2 and the tetragonal phase of ZrO_2 in the mixture. However, all three samples TS9, TT9, TZ9 prepared by the impregnation method (Figure 3.37B) have peaks typical for the monoclinic phase of WO_3.

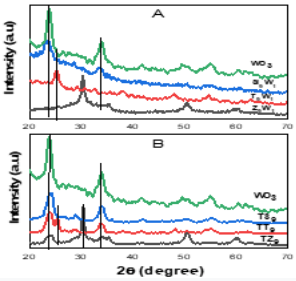

Figure 3.37. Wide-angle XRD pattern of Me_9W_1 (Me: Si, Ti, Zr) (A) and comparison WO_3/MeO_2 material samples (B)

Thus, with the same ratio W/Me=1/9, in the impregnation method, WO_3 can only be dispersed on the surface of MeO_2 carriers (also prepared by the solgel method above).

3.4.3. STEM-HAADF image of Me_9W_1 material (M = Si, Ti, Zr).

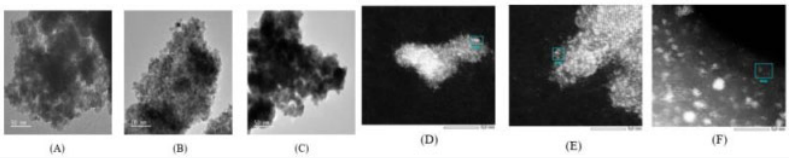

Figure 3.38. STEM and STEM-HAADF images of materials Zr-W-O (A, D), Ti-W-O (B, E), Si-W-O (C, F).

Figure 3.38 shows that the catalysts are all composed of nanoparticles with a diameter of 4-8nm. The particle size of the Ti_9W_1 and Zr_9W_1 catalysts is slightly larger than that of the Si_9W_1 catalyst. In the STEM–HAADF image, the bright regions correspond to the WO_x phase because W is the heaviest element in the mixed oxides. For the Zr_9W_1 catalyst, it can be seen that besides single WO_x monotungstates, WO_x nanoclusters account for a fairly large proportion. Similar results were observed with the Ti_9W_1 catalyst, with multiple WO_x nano-cluster sites consisting of several W atoms. The Si_9W_1 sample shows bright spots with diameters ranging from ca. 1-3 nm, corresponding to WO_x nanoclusters. Compared with the cases of Zr_9W_1 and Ti_9W_1, the WO_x nanoclusters on Si_9W_1 are larger and more clearly separated.

3.4.4. N_2 adsorption-desorption isotherm and acid properties of Me_9W_1 material (Me = Si, Ti, Zr).

The N_2 adsorption and desorption isotherm and pore size distribution curve of Me_9W_1 material (Me: Si, Ti, Zr) are presented in Figure 3.39. Their TPD-NH_3 diagram is shown in Figure 3.40.

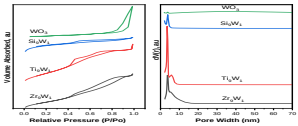

Figure 3.39. N_2 adsorption and desorption isotherm (A) and pore size distribution curve of Me_9W_1 material (Me: Si, Ti, Zr) (B)

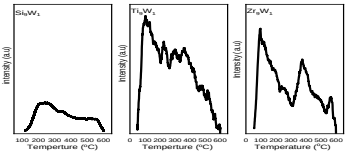

Figure 3.40. TPD-NH_3 diagram of Me_9W_1 material (Me: Si, Ti, Zr)

Table 3.8 shows that Me_9W_1 material (Me: Si, Ti, Zr) has a large surface area and large average pore diameter, which is favorable for the diffusion of reactants to the catalyst surface. work.

Table 3.8. Some morphological and surface properties of Me_9W_1 catalyst (Me: Si, Ti, Zr)

Mẫu	S_{BET} (m^2/g)	V_{pore} (cm^3/g)	D_{BJH} (nm)	Lượng NH_3 (mmol/$g_{xúc\ tác}$)				W^{5+}/W^{6+}	Hiệu suất tạo 5-HMF
				Acid yếu (150-300°C)	Acid trung bình (300-500°C)	Acid mạnh (> 500°C)	Tổng lượng tâm acid		
WO_3	25,5	30,5	0,17	0.131	0.169	0.008	0.308	--	58,1
Zr_9W_1	106,4	0,137	5,20	0.333	0.401	0.035	0.769	0,48	95,8
Ti_9W_1	148,4	0,144	3,89	0.303	0.217	0.059	0.578	0,30	84,0
Si_9W_1	173,4	0,046	4,33	0.287	0.424	0.074	0.785	0,09	84,3

Thus, the Me_9W_1 materials show significantly higher NH_3 desorption capacity than the WO_3 sample. The presence of well-dispersed WO_3 clusters on MeO_2 produces a higher number of weak to moderately acidic sites. This fact shows that the introduction of WO_3 into the MeO_2 structure leads to a significant increase in the concentration of medium acid sites, which contributes to improving the catalyst activity.

3.4.5. Comparison of catalytic efficiency

The effectiveness of the catalysts was evaluated through the conversion of fructose into 5-HMF with different reaction conditions: reaction temperature, reaction time and fructose content.

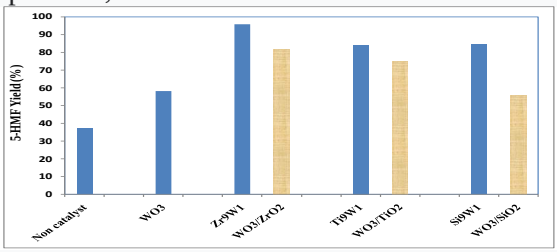

Figure 3.41. HMF performance on Me_9W_1 catalyst (Me: Si, Ti, Zr) and WO_3/MeO_2 synthesized by impregnation method.

Comparison results show that among Me-O-W oxides, Zr_9W_1 catalyst has the highest 5-HMF formation efficiency, reaching

95.8%. Following the Zr_9W_1 catalyst are Ti_9W_1 and Si_9W_1 with approximately equal 5-HMF efficiency, reaching 84%. In addition, it can be seen that, compared to the WO_3 catalyst and the mixed catalyst synthesized by the WO_3/MeO_2 impregnation method, the Me-O-W mixed catalyst shows superior activity.

To evaluate this difference in Me-O-W catalysts, the material surface properties need to be compared. It can be seen that the catalytic activity is not proportional to the specific surface area on which the active phase is dispersed of the material, but seems to be proportional to the amount of weak acid site; 0.333 mmol/gxt (Zr_9W_1) > 0.303 (Ti_9W_1 > 0.287 mmol/gxt (Si_9W_1). These are the centers corresponding to NH_3 desorption in the temperature range of 150-300^oC, close to the investigated temperature range of the reaction. Side Besides, it is also found that the average pore diameter of the capillary catalyst can play an important role in the diffusion of reactants. From this perspective, it is clear that the Zr_9W_1 catalyst (porous = 5.20 nm) shows superiority over Ti_9W_1 (pore size = 3.89 nm) and Si_9W_1 (pore size = 4.33 nm) catalysts (Table 3.6). In addition, it should be noted that, XPS results show that the ratio of acid centers assigned to W^{5+}-OH bronsted centers to W^{6+}=O Lewis centers is very high on Zr_9W_1 catalyst, reaching 0.48, while on Ti_9W_1 and Si_9W_1 catalysts it is only 0.30 and 0.09. All of these properties create an additive effect that greatly increases the efficiency of 5-HMF generation on Zr_9W_1 catalyst.

The strong increase in activity of Me-O-W mixed oxide with low W content (W/Me = 1:9) has also been shown in some previous studies due to the formation of nanoclusters containing active centers. high character. Studies have shown that when the W content is low, with a W surface density in the range of 4-8W/nm^2, the isolated nanocluster structure occupies a large part and is considered the structure containing the highest active center of the phase. WO_3 crystal. In our case, based on XPS analysis, the surface density W is 4,3; 9,7; 7.3 W/nm^2 for Zr_9W_1, Ti_9W_1, Si_9W_1 . These values are quite close to the surface density W with the highest catalytic activity mentioned above. High catalytic activity at low W content was also observed on Nb-O-W catalysts for the hydrolysis of sucrose and the hydration of glucose and mannose.

3.5. Proposed mechanism for the dehydration reaction of fructose to 5-HMF

Stage 1, splitting the first water molecule creates an intermediate product (1). The reactions are presented in Figure 3.42.

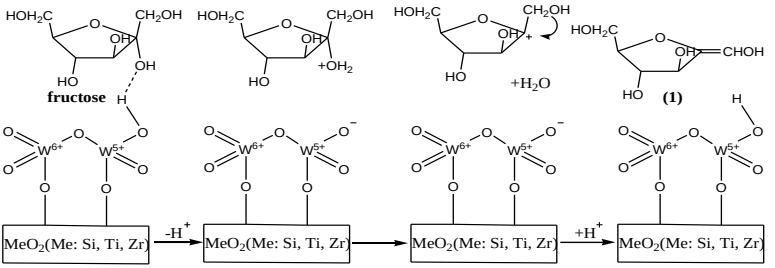

Figure 3.42. Mechanism for separating the first water molecule from fructose

Stage 2, splits the second water molecule to create an intermediate product (2). The reactions are presented in Figure 3.43.

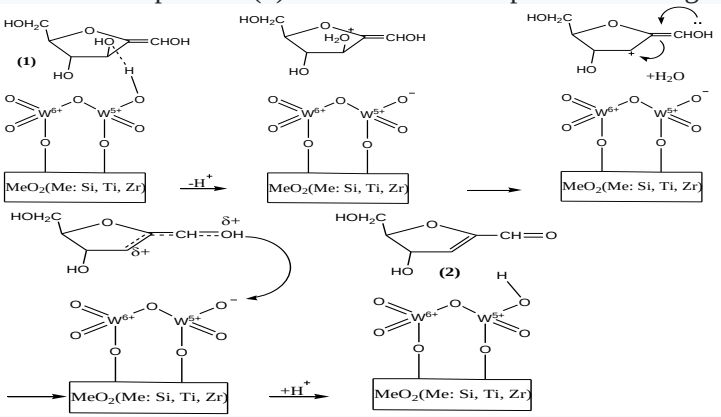

Figure 3.43. Second water molecule splitting mechanism

Stage 3, splitting the third water molecule produces the final product 5-HMF. The reactions are presented in Figure 3.44.

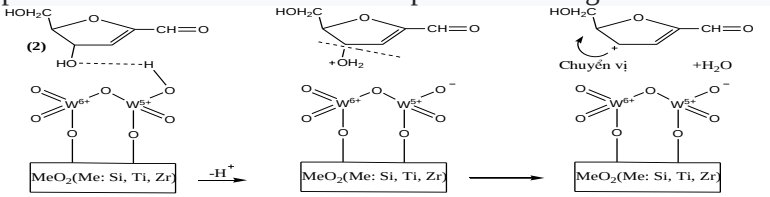

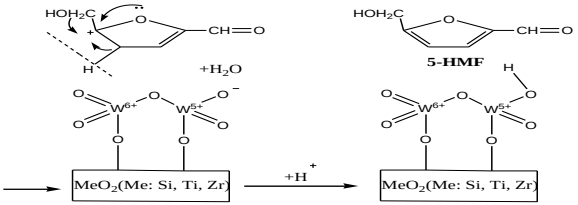

Figure 3.44. The third water molecule splitting mechanism forms 5-HMF

Thus, in Me-O-W catalytic materials, the Bronsted acid center plays the role of donating H^+ protons to fructose to perform the dehydration process into 5-HMF.

CONCLUDE

1) Si-O-W, Ti-O-W and Zr-O-W catalysts were successfully synthesized by sol-gel method. The XRD pattern shows that WO_3 exists in Si-O-W catalyst, anatase TiO_2 in Ti-O-W and tetragonal ZrO_2 in Zr-O-W in the structure when heated at 400°C. From SEM, TEM, and HRTEM-HAADF results, it shows that the WO_x phase is uniformly dispersed on the material surface and the WO_x has a diameter of less than 2.5 nm. XPS spectrum shows the existence of W^{6+}, W^{5+} for the catalysts. The TPD-NH_3 spectrum shows a strong increase in the number of acid centers in Me-W-O mixed oxides.
2) In the Si-O-W, Ti-O-W and Zr-O-W catalyst systems, the Si_9W_1, Ti_9W_1 and Zr_9W_1 catalysts show high activity in the synthesis of 5-HMF from fructose, with respectively are 84.4%, 84% and 95.8%. The conversion efficiency of fructose into 5-HMF of mixed oxide samples is significantly higher than that of individual oxide samples, due to the resonance effect between the two oxide phases MeO_2 and WO_x, especially the dispersion of WO_x nanoclusters. on MeO_2 background phase. Factors affecting the conversion efficiency of fructose into 5-HMF such as Me/W ratio, temperature, time, fructose concentration, and reaction solvent were investigated. Optimal reaction conditions in the reaction to convert fructose to 5-HMF: reaction time 2 hours, reaction temperature 120°C, fructose concentration 5% by weight and solvent DMSO. The material samples Si_9W_1, Ti_9W_1 and Zr_9W_1 have almost constant activity after 3 reaction cycles.
3) Compared with WO_3 oxide catalyst, Si_9W_1, Ti_9W_1 and Zr_9W_1 catalysts show superior activity, especially in the case of Zr_9W_1

catalyst. Zr_9W_1 catalyst has the highest conversion efficiency of fructose into 5-HMF (95.8%). This result is shown to be compared to the combination of favorable properties obtained on the Zr_9W_1 catalyst such as; the increase in acid center, wider capillary diameter favorable for diffusion and clear and even dispersion of nanocluster structures on ZrO_2 substrate. These superior properties on the Zr_9W_1 catalyst have shown the superiority of the solgel method in synthesizing WO_x-based catalysts for the conversion of fructose to 5-HMF.

NEW CONTRIBUTIONS OF THE THESIS

1. Me-O-W mixed oxide catalysts (Me: Zr, Ti, Si) with different Me/W ratios were successfully synthesized for the first time by the sol-gel method with precursors WCl_6 and $Si(OC_2H_5)_4$, $Ti(OC_4H_9)_4$, $ZrOCl_2$.
2. Structural characterization analyses have revealed the formation of well-dispersed WO_x nanoclusters, with diameters ranging from 1 to 2 nanometers, achieved through the utilization of the sol-gel method. Notably, this uniform dispersion is particularly pronounced in the case of the Zr_9W_1 catalyst, where agglomeration into larger particles is conspicuously absent. The study also showed the advantage of forming nanocluster phases on the oxide base using sol-gel method compared to the catalysts prepared by conventional impregnation method.
3. The conversion of fructose into hydroxymethylfurfural (HMF) using Me-W-O catalysts was systematically studied. As the results, Zr_9W_1 synthesized using sol-gel method shows exceptionally high HMF conversion (95.8%), outperformed the catalytic activity of the impregnation method prepared counterpart (only 81.6%). Surprisingly, the HMF conversion performance of sol-gel synthesized Zr_9W_1 surpasses the previously reported catalysts.
4. The optimal HMF conversion reaction condition is investigated. The optimized condition is 5 wt% of fructose in DMSO solvent with the presence of 100 mg of catalyst at 120^{o}C for 2 hours.

LIST OF PUBLISHED SCIENTIFIC WORKS

I. Articles

1. Pham Thi Hoa, Nguyen Ngoc Anh, Nghiem Thi Thuy Ngan, Chu

Ngoc Chau, Dang Thi Thuy Hanh, Nguyen Thi Ngoc Quynh, Nguyen Thanh Binh, *Synthesis of Ti-W oxide catalyst and evaluation of activity in the reaction Conversion of fructose to 5-hydroxymethylfurfural*, Chemical Journal, volume 57, number 4e1,2, pages 40–44, 2019.

2. Pham Thi Hoa, Chu Ngoc Chau, Nguyen Ngoc Anh, Dang Thi Thuy Hanh, Nguyen Thi Ngoc Quynh, Nguyen Thanh Binh, *Synthesis and evaluation of Zr - W oxide catalytic activity in the reaction of converting fructose into 5 - hydroxymethylfurfural*, Journal of Chemistry, volume 57, number 4e3,4, pages 131–135, 2019.
3. Pham Thi Hoa, Nghiem Thi Thuy Ngan, Nguyen Ngoc Anh, Dang Thi Thuy Hanh, Do Van Dang, Nguyen Thi Ngoc Quynh, Nguyen Thanh Binh, *Synthesis, characterization and catalytic activity estimation of Si-W-O oxides for fructose conversion reaction into 5-hydroxymethylfurfural*, Vietnam J. Chem., 2020, 58(5E12), 415-419.
4. Pham Thi Hoa, Pham Thi Thanh Ngan, Nguyen Thanh Binh, *Research on the synthesis of some WO3/MeO2 oxide catalysts (Me: Zr, Ti, Si) and evaluation of catalytic activity in the reaction of converting fructose into 5-hydroxymethylfurfural*, Vietnam Journal of Catalysis and Adsorption, volume 10, number 3, pages 78-81, 2021.
5. Hoa Pham Thi, Doan Pham Minh, Ngoc Quynh Nguyen Thi, Thanh-Binh Nguyen, *Efficient conversion of fructose into 5-hydroxymethylfurfural on W-Zr-O catalyst: role of single and sub nanocluster for the catalytic performance(Submitted to Reaction).*
6. Hoa Pham Thi, Doan Pham Minh, Ngoc Quynh Nguyen Thi, Thanh-Binh Nguyen, *High active site nano WO_3 cluster in mixed oxides Me-W-O (Me: Si, Zr, Ti) for efficient conversion of fructose to 5-hydroxymethylfuifural (Submit to Chemical Engineering Technology).*

II. Report in the Conference:

1- Pham Thi Hoa, Nghiem Thi Thuy Ngan, Nguyen Thi Ngoc Quynh, Nguyen Thanh Binh, *"Synthesis, characterization and catalytic activity estimation of Si_xW_{10-x} oxides for fructose conversion reaction into 5- hydroxymethylfurfu*ral*",*the 3rd RoHan Summerschool, 09th-21th September 2019, Rohan catalysis, SDG graduate school.